

Improvement direct torque control of induction motor using robust intelligence artificial ANFIS speed controller

Laoufi Abdelhaq^{1,2}, Chergui Moulay-Idriss¹, Soufiane Chekroun¹

¹Department of Electrical Engineering, Faculty of Sciences and Technology, University Mustapha Stambouli of Mascara, Mascara, Algeria

²Signals and Systems Laboratory, Faculty of Sciences & Technology, University Abdelhamid Ibn Badis of Mostaganem, Mostaganem, Algeria

Article Info

Article history:

Received Aug 5, 2024

Revised May 30, 2025

Accepted Jul 23, 2025

Keywords:

ANFIS
Direct torque control
Fuzzy logic
Induction motor
PI

ABSTRACT

This paper proposes a study aimed at improving the conventional direct torque control (DTC) technique applied to induction motors (IM). The primary aim is to reduce the harmonic distortions and fluctuations associated with the electrical current, flux variations, and generated torque, while ensuring accurate speed reference tracking and ensuring optimal dynamic performance of the drive, especially under variable speed conditions. To achieve this, we introduce an intelligent control system that utilizes a hybrid neuro-fuzzy inference model (ANFIS), through the application of the back propagation method. The DTC-ANFIS technique is compared with the traditional DTC-PI method and simulated using MATLAB/Simulink in different scenarios. The obtained results reveal a significant improvement in performance over DTC-PI, with superior results over a wide speed range.

This is an open access article under the [CC BY-SA](https://creativecommons.org/licenses/by-sa/4.0/) license.



Corresponding Author:

Laoufi Abdelhaq
Department of Electrical Engineering, Faculty of Sciences and Technology
University Mustapha Stambouli of Mascara
BP. 305, Route El Mamounia, Mascara 29000, Algeria
Email: abdelhaq.laoufi@univ-mascara.dz

NOMENCLATURE

T_e, T_r	: Electromagnetic torque and resistance	L_s, L_r	: Stator and rotor inductances
i_{ds}, i_{qs}	: Stator current	L_m	: Mutual inductance
i_{dr}, i_{qr}	: Rotor currents	p	: Number of pole pairs
Φ_{ds}, Φ_{qs}	: Stator flux	J	: Moment of inertia
Φ_{dr}, Φ_{qr}	: Rotor flux	f	: Friction coefficient
ω_s	: Stator angular electrical speed	S_a, S_b, S_c	: Sequence of the DTC
R_s, R_r	: Stator and rotor resistances	E, v_{dc}	: The DC voltage of the battery
V_A, V_B, V_C	: Inverter output voltages		

1. INTRODUCTION

Since the 1950s, with the first advances in artificial intelligence [1], [2], the demand for labor in sectors such as manufacturing, farming, and service industries has gradually reduced. In particular, artificial intelligence [3], [4], a subfield of computer science, focuses on the creation of systems designed to process data, learn from it, and generate predictions or decisions based on the insights gained. This technology, oriented towards prediction, makes it possible to process large amounts of information and generate useful predictions, thus offering concrete and rapid solutions. This study explores different types of intelligent

controls, and we will specifically implement a hybrid command technique using a neuro-fuzzy inference model (ANFIS) to enhance the performance of direct torque control (DTC) applied to induction machines [5].

ANFIS control was developed through the combination of two intelligent control approaches: neural network with fuzzy logic. This merged framework, built upon both artificial neural models and fuzzy reasoning mechanisms, takes advantage of the respective strengths of each method [6]. In this structure, the neural component is responsible for deriving fuzzy rules from input data, while the fuzzy sets are continuously refined during the training phase. The supervised learning algorithm allows the neuro-fuzzy networks to learn complex relationships by analyzing sets of examples composed of inputs and their corresponding outputs [7]. With this hybrid method, ANFIS connects inputs and outputs using a supervised learning technique, while integrating human expertise to refine the results.

Introduced by Takahashi in 1985, the DTC technique is characterized by its simplicity of implementation and its efficiency [8]. Many works have made it possible to specify and refine the modelling of this approach [8], [9]. DTC allows determining the control quantities, such as the stator flux and the produced torque, only from the readings of the stator currents, without using mechanical sensors. In its basic structure [10]. This technique directly selects a voltage vector from a commutation table, in accordance with the principle of direct control, in order to regulate the converter. This mechanism ensures a fast torque response.

However, this method also has some drawbacks. The use of hysteresis controllers allows maintaining the torque and stator flux errors within acceptable bounds, but it generates a significant torque ripple [11], [12]. Other limitations of conventional DTC include high torque ripple, average torque that may not match the exact demand, and variable switching frequency, which may affect the overall system performance.

To overcome these limitations, researchers have suggested many control techniques, including nonlinear strategies, advanced methods, and artificial intelligence approaches, all aiming to enhance the effectiveness of conventional DTC [11], [13]. In this study, we explored and developed an intelligent control approach using the hybrid neuro-fuzzy inference model applied to DTC for asynchronous motors. To evaluate the reliability of this technique, we carried out a comparison of this technique and the conventional DTC with a PI controller.

2. METHOD

2.1. Modelling of IM

To monitor and regulate the behavior of the induction machine, a mathematical model is necessary. For this purpose, we have defined the state vector, which consists of the electrical currents in the stator (i_{ds}, i_{qs}), and the magnetic flux in the rotor (ϕ_{ds}, ϕ_{qs}) [14]. The complete model of the asynchronous machine is expressed as (1) [15], [16].

$$\begin{cases} \frac{di_{ds}}{dt} = \frac{1}{\sigma L_s} \left[-\left(R_s + \left(\frac{L_m}{L_r}\right)^2 R_r\right) i_{ds} + \sigma L_s \omega_s i_{qs} + \frac{L_m R_r}{L_r^2} \phi_{dr} + \frac{L_m}{L_r} \phi_{qr} \omega + V_{ds} \right] \\ \frac{di_{qs}}{dt} = \frac{1}{\sigma L_s} \left[-\sigma L_s \omega_s i_{ds} - \left(R_s + \left(\frac{L_m}{L_r}\right)^2 R_r\right) i_{qs} - \frac{L_m}{L_r} \phi_{dr} \omega + \frac{L_m R_r}{L_r^2} \phi_{qr} + V_{qs} \right] \\ \frac{d\phi_{dr}}{dt} = -\frac{L_m R_r}{L_r} i_{ds} - \frac{R_r}{L_r} \phi_{dr} + (\omega_s - \omega) \phi_{qr} \\ \frac{d\phi_{qr}}{dt} = -\frac{L_m R_r}{L_r} i_{qs} - \frac{R_r}{L_r} \phi_{qr} - (\omega_s - \omega) \phi_{dr} \\ \frac{d\omega}{dt} = \frac{p^2 L_m}{L_r J} (\phi_{dr} i_{qs} - \phi_{qr} i_{ds}) - \frac{f}{J} \omega - \frac{P}{J} T_r \end{cases} \quad (1)$$

Where σ the coefficient of dispersion is $\sigma = 1 - \frac{L_m^2}{L_s L_r}$.

2.2. Two-level voltage inverter model

A three-phase inverter functions as a static DC-AC converter capable of generating three symmetrical output voltages with controllable amplitude and frequency. In the modeling process, the converter is treated as a two-level voltage source inverter VSI-2L [17], Figure 1 represents the equivalent schematic of a two-level three-phase voltage inverter used to supply an asynchronous motor. This diagram highlights the power conversion structure and the operating principle of the inverter. The mathematical model of a two-level voltage inverter presented by [17], [18].

$$\begin{bmatrix} V_A \\ V_B \\ V_C \end{bmatrix} = \frac{E}{3} \begin{bmatrix} 2 & -1 & -1 \\ -1 & 2 & -1 \\ -1 & -1 & 2 \end{bmatrix} \begin{bmatrix} S_a \\ S_b \\ S_c \end{bmatrix} \quad (2)$$

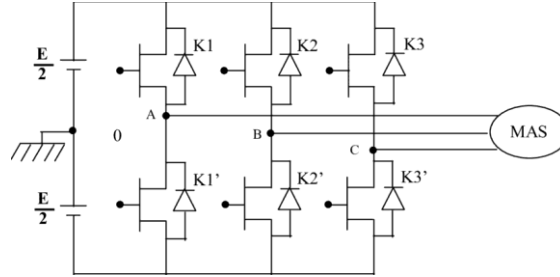


Figure 1. Voltage source inverter

2.3. Principle of traditional direct torque control

Figure 2 illustrates the fundamental structure of the traditional DTC drive, as proposed by Takahashi. This diagram highlights the control architecture and the main components involved in torque and stator flux regulation. It includes the following fundamental components: torque and flux estimators, a set of hysteresis controllers, a sector calculation unit, and a look-up table for optimal switching vectors [19], [20].

$$\begin{cases} \varphi_s(t) = \int_0^t (V_s - R_s \bar{I}_s) dt = \Delta \bar{\varphi}_s = \bar{v}_s T_e \\ T_e = p(\varphi_{\alpha s} I_{\beta s} - \varphi_{\beta s} I_{\alpha s}) \end{cases} \quad (3)$$

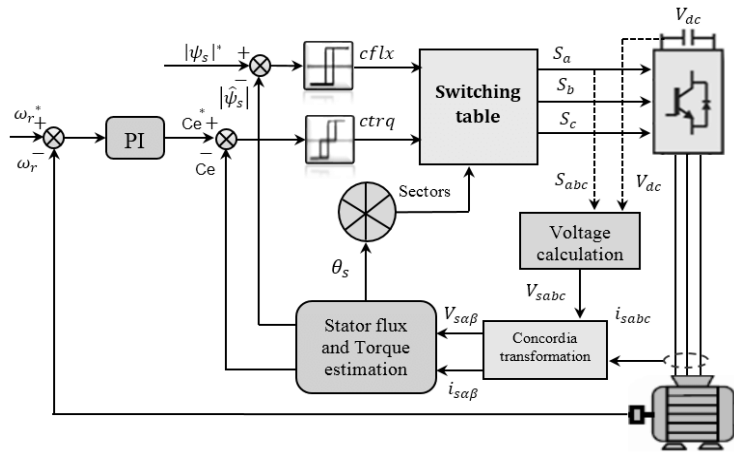


Figure 2. Traditional DTC-based PI controller for an induction machine

2.3.1. Estimator for electromagnetic torque and magnetic flux

Before approaching the study of the flux controller, we define the computational steps necessary to estimate the stator flux amplitude. Thus, from the (4), we will establish the decomposition of the flux vector $\bar{\varphi}_s$ along the axes (α_s, β_s) either [15], [21].

$$\bar{\varphi}_s = \varphi_{\alpha s} + j\varphi_{\beta s} \quad (4)$$

$$\begin{cases} \varphi_{\alpha s} = \int_0^t (V_{\alpha s} - R_s I_{\alpha s}) dt \\ \varphi_{\beta s} = \int_0^t (V_{\beta s} - R_s I_{\beta s}) dt \end{cases} \quad (5)$$

The compound voltages $V_{\alpha s}$ and $V_{\beta s}$ of V_s obtain from the measured input voltage of the inverter U_c , the control situation of S_a, S_b , and S_c , by applying the Concordia transformation, we obtain [22]:

$$\overline{V_s} = V_{ds} + jV_{qs} \quad (6)$$

$$\begin{cases} V_{ds} = \sqrt{\frac{2}{3}} U_c (S_a - \frac{1}{2}(S_b + S_c)) \\ V_{qs} = \frac{1}{\sqrt{2}} U_c (S_b - S_c) \end{cases} \quad (7)$$

The currents $I_{\alpha s}, I_{\beta s}$ are also obtained by the Concordia transformation, from the measured currents $I_{a s}, I_{b s}, I_{c s}$ either [13].

$$\overline{I_s} = I_{\alpha s} + jI_{\beta s} \quad (8)$$

$$\begin{cases} I_{\alpha s} = \sqrt{\frac{2}{3}} U_c I_{as} \\ I_{\beta s} = \sqrt{\frac{2}{3}} (I_{bs} - I_{cs}) \end{cases} \quad (9)$$

The modulus of the stator flux is (10).

$$\varphi_s = \sqrt{\varphi_{\alpha s}^2 + \varphi_{\beta s}^2} \text{ and } \theta_s = \tan^{-1} \frac{\varphi_{\beta s}}{\varphi_{\alpha s}} \quad (10)$$

From the expression of the electromagnetic torque, we can estimate the torque T_e only from the stator magnitudes flux $\varphi_{\alpha s}, \varphi_{\beta s}$ and currents $I_{\alpha s}, I_{\beta s}$. We then obtain the following form of the torque:

$$T_{em} = p(\varphi_{\alpha s} I_{\beta s} - \varphi_{\beta s} I_{\alpha s}) \quad (11)$$

2.3.2. Hysteresis controllers for electromagnetic torque and magnetic flux

The deviation between the reference stator flux and the estimated stator flux is managed using a two-stage hysteresis controller that generates the latter 0 or 1 following the (9) and (10) [23].

$$H_\varphi = 1 \text{ if } \Delta\varphi \leq |\varphi^*| - |\varphi_s| \quad (12)$$

$$H_\varphi = 0 \text{ if } \Delta\varphi \leq |\varphi^*| + |\varphi_s| \quad (13)$$

The difference between the reference torque and the estimated torque is controlled in a three-level hysteresis controller that generates the latter -1 or 1 or 0 following the (14)-(16) [23].

$$H_{T_e} = 1 \text{ if } \Delta T_e < |T_e^*| - |T_e| \quad (14)$$

$$H_{T_e} = -1 \text{ if } \Delta T_e < |T_e^*| + |T_e| \quad (15)$$

$$H_{T_e} = 0 \text{ if } |T_e^*| - |T_e| < \Delta T_e < |T_e^*| + |T_e| \quad (16)$$

2.3.3. Sector selection and switching table

The truth table for the check structure is developed using the outputs of the checkers and the N field locations φ_s such that:

$$\theta = \text{Arctan} \left(\frac{\varphi_{\beta s}}{\varphi_{\alpha s}} \right) \quad (17)$$

The space of evolution of φ_s in the considered reference frame is decomposed in 6 zones N (1 to 6). This choice is dictated by a concern for a more rigorous control and such that:

$$-\frac{\pi}{6} + (N-1)\frac{\pi}{3} \leq \theta < \frac{\pi}{6} + (N-1)\frac{\pi}{3} \quad (18)$$

Table 1 applies the switching table as introduced by the selected voltage vector, which is decomposed and then applied to the voltage source inverter [24]. Table 2 shows the sequence of the DTC command applied directly to the voltage inverter. By selecting one of the two null vectors \vec{V}_0 or \vec{V}_7 . The rotation of the flux φ_s stop and results in a decrease in the torque T_{em} . Alternatively, \vec{V}_0 or \vec{V}_7 is chosen to minimize the number of switches on the inverter.

$$V_s = \sqrt{\frac{2}{3}} U_c \left[S_a + S_b e^{j\frac{2\pi}{3}} + S_c e^{j\frac{4\pi}{3}} \right] \quad (19)$$

Table 1. Takahashi vector selection table [25]

N	1	2	3	4	5	6
$H_{Te} = 1$	$H_\varphi = 1$	V_2	V_3	V_4	V_5	V_6
	$H_\varphi = 0$	V_7	V_0	V_7	V_0	V_7
	$H_\varphi = -1$	V_6	V_1	V_2	V_3	V_4
$H_{Te} = 0$	$H_\varphi = 1$	V_3	V_4	V_5	V_6	V_1
	$H_\varphi = 0$	V_0	V_7	V_0	V_7	V_0
	$H_\varphi = -1$	V_5	V_6	V_1	V_2	V_3

Table 2. Voltage vector generation mode

V_1	V_2	V_3	V_4	V_5	V_7
0°-	60°-	120°-	180°-	240°-	300°-
60°	120°	180°	240°	300°	360°
S_1	S_2	S_3	S_4	S_5	S_6
S_6	S_1	S_2	S_3	S_4	S_5
S_5	S_6	S_1	S_2	S_3	S_4
101	100	110	010	011	001

2.4. Design of fuzzy logic controller

In order to control or study a physical system, it is necessary to construct a mathematical model, knowing that all physical systems are non-linear. Unless we can apply the principles of physics, it becomes challenging to develop an accurate non-linear model from measurement data and system identification methods. What's more, It is frequently too complicated to implement in controller development [26]-[28].

Alternatively, fuzzy control offers a structured approach to represent and apply a human-like control model [26]. It employs only a small subset of fuzzy mathematics, which is not only mathematically simple but also conceptually accessible. Figure 3 provides a detailed analysis of the fundamental notions, vocabulary, and calculations of fuzzy sets and fuzzy logic. The fuzzy controller structured around four main components that define its architecture and operating mechanism [29], [30]:

- The fuzzification block transforms the crisp inputs into fuzzy values that can be matched against the stored rules.
- The knowledge base contains a collection of fuzzy rules that encapsulate the control strategy.
- The inference engine determines which rules are applicable based on the current inputs and computes the appropriate fuzzy outputs.
- The defuzzification block translates the fuzzy outputs generated by the inference engine into precise control actions sent to the system [28], [29].

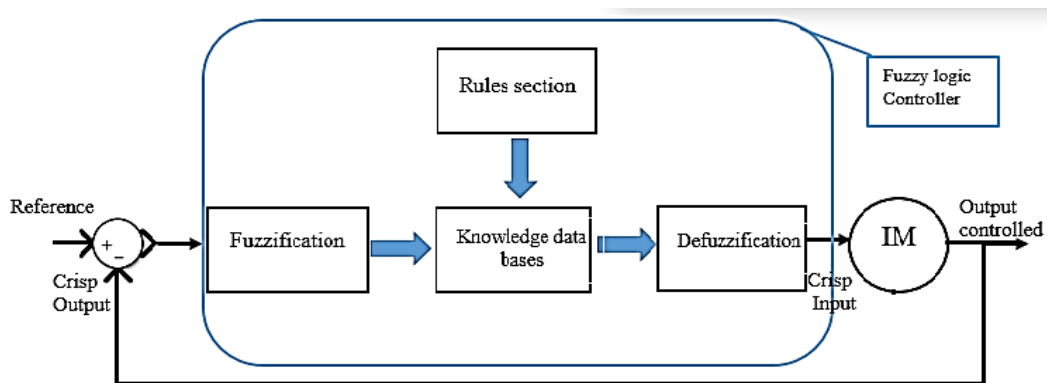


Figure 3. Fuzzy logic controller structure

2.5. Design of ANFIS controller

The ANFIS represents a hybrid intelligent approach that unifies fuzzy logic reasoning with the self-learning ability of neural networks. This paradigm allows optimizing the performance of intelligent systems

by integrating the knowledge acquired during the learning process [25], [27]. This system uses a first-order Takagi-Sugeno-Kang fuzzy model, which first generates an initial fuzzy system. The ANFIS controller takes the error and its rate of change as inputs. To optimize system performance and drive the error to zero, adaptive learning techniques are employed to adjust the parameters dynamically. During the inference and rule-definition phase, a back-propagation method is employed to fine-tune the structure of the neural network, allowing it to enhance the rule base and create fuzzy logic functions for both inputs as well as outputs. The input membership functions of the fuzzy logic controller related to the speed error (e) and the change in speed error (de) are shown in Figures 4(a) and 4(b), respectively, while the output membership functions of the fuzzy controller are illustrated in Figure 4(c). The along with associated fuzzy rules can be found in Table 3. Such a process depends on a meticulously filtered dataset, ensuring high accuracy and optimal computational efficiency [31], [32]. Figure 5 illustrates an overall architecture describing the ANFIS neuro-fuzzy system, as introduced by Jang, based on a flexible network that combines the characteristics of fuzzy inference systems with adaptive learning mechanisms, making it a powerful tool for various intelligent applications [30], [31].

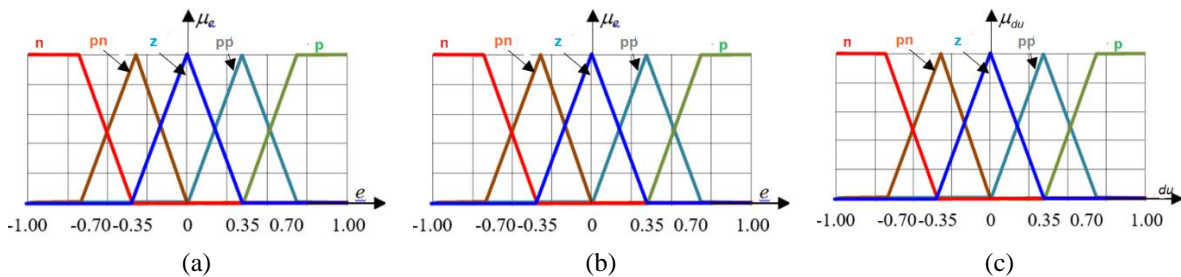


Figure 4. ANFIS controller membership functions: (a) input speed error e , (b) change in speed error de , and (c) output membership du

Table 3. Rule-based learning algorithm to elaborate ANFIS

$\begin{matrix} E \\ dE \end{matrix}$	n	pn	z	pp	p
n	n	N	pn	pn	z
pn	n	pn	pn	z	p
z	n	pn	z	pp	p
pp	n	z	pp	pp	p
p	z	pp	pp	p	p

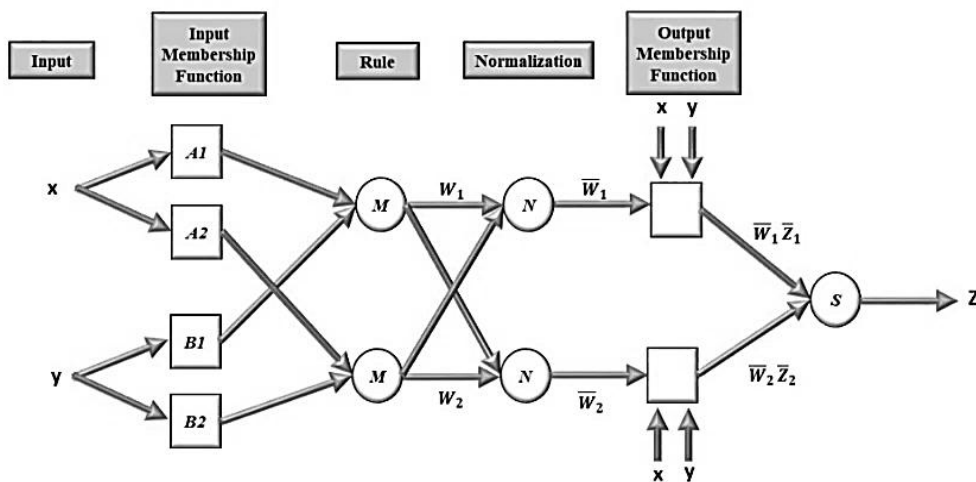


Figure 5. Global architecture for neuro-fuzzy ANFIS [33]

In this system, A1, A2, and B1, B2 represent fuzzy collections within the premise part, The parameters p_i and q_i are configuration coefficients adjusted throughout the training phase. The structure of the ANFIS model includes five distinct layers, detailed below [34]:

- Layer 1: This initial layer, referred to as the fuzzification layer, transforms crisp inputs into fuzzy values. Each node's output in this layer is calculated using the following expression (13) [35]:

$$O_i^1, i = \mu_{A_i}(x) = \exp\left(-\left(\frac{x-c_i}{\sigma_i}\right)^2\right) \quad (13)$$

Where: i is the index of the membership function, x is the input to the node, and $\{\sigma_i, b_i, c_i\}$ are the initial parameters defined at the start of the training process.

- Layer 2: In this layer, each node computes the firing strength of a rule. The output of node i is calculated using (14):

$$O_i^2 = w_i = \mu_{A_i}(x_1) \cdot \mu_{B_i}(x_2), i = 1, 2 \quad (14)$$

- Layer 3: Responsible for normalizing the firing strengths of the rules, this stage produces a normalized value at node i , computed using the (15) [35]:

$$\bar{w}_i = \frac{w_i}{\sum_{k=1}^n w_k} \quad (15)$$

- Layer 4: This layer is responsible for defuzzification and generating the results. At each node, the weighted results of the corresponding rule are computed. The (16) is used to calculate these values [36].

$$O_{4i} = \bar{w}_i f_i = \bar{w}_i (p_i x + q_i y + r_i). \quad (16)$$

To fine-tune parameters within the ANFIS model, the least squares and back-propagation methods are used jointly. Figure 6 presents the results of the training step, where five Gaussian membership functions are applied for the DTC-ANFIS [37].

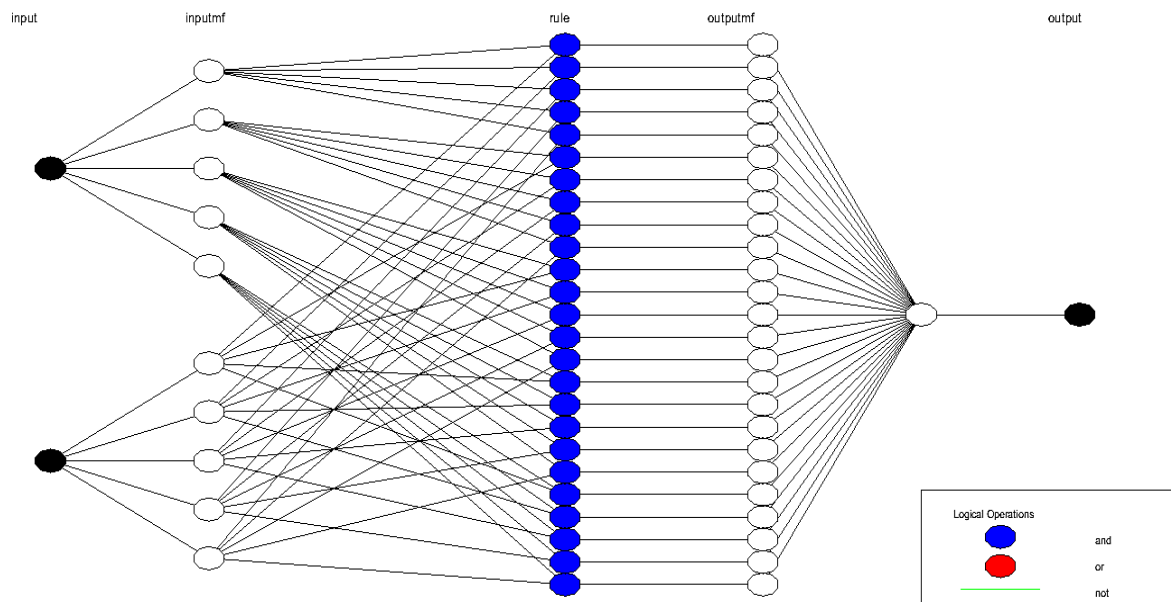


Figure 6. Network structure for DTC-ANFIS

3. RESULTS AND DISCUSSION

To accurately simulate the system's behavior, we modeled the desired circuit using MATLAB simulation software. The global block is structured into two main blocks: direct torque control and the

asynchronous motor, as demonstrated in Figure 7. Figure 8 presents a close-up of the Simulink model of the induction motor, highlighting its key components, such as the mathematical model, the electrical and mechanical equations, and the interactions between the stator and rotor phases. Similarly, Figure 9 presents in detail the Simulink model of the DTC control, encompassing torque and flux regulation, optimal voltage vector selection, as well as the two-level inverter model, ensuring precise and effective motor control.

In this section of our study, we conduct analysis and comparison tests through MATLAB Simulink. The parameters of the induction machine and the dual-level voltage inverter used in the simulation are summarized in Table 4. The inverter operates with a DC voltage of 500 V and a switching frequency of 10 kHz. These parameters serve as the reference for evaluating the efficiency and behavior of the DTC controller integrated with the ANFIS controller. These experiments aim to validate the overall system performance and demonstrate its robustness.

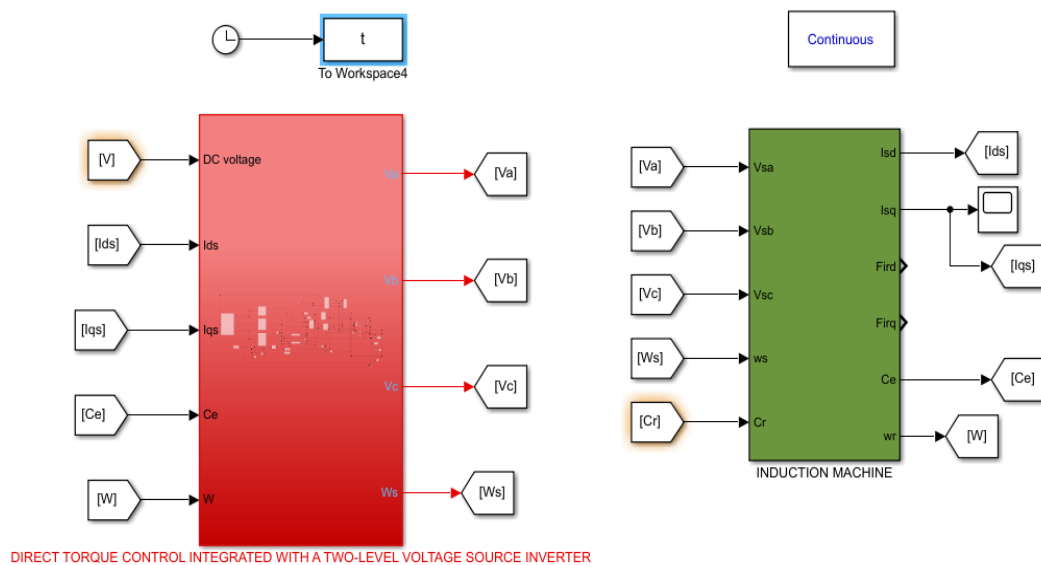


Figure 7. Global block diagram illustrating direct torque control (DTC) applied to an IM in MATLAB/Simulink

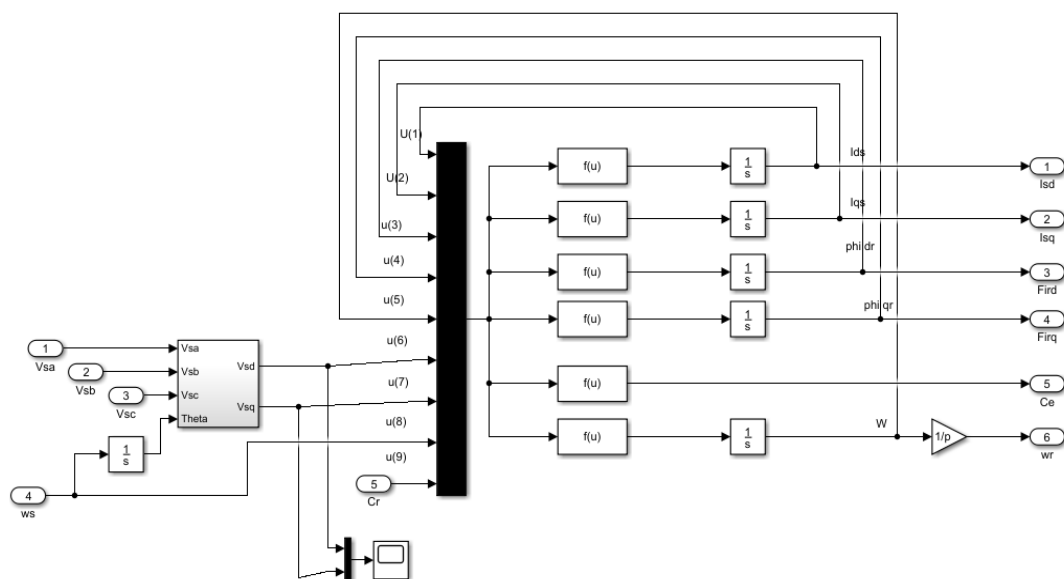


Figure 8. Induction machine model in MATLAB/Simulink

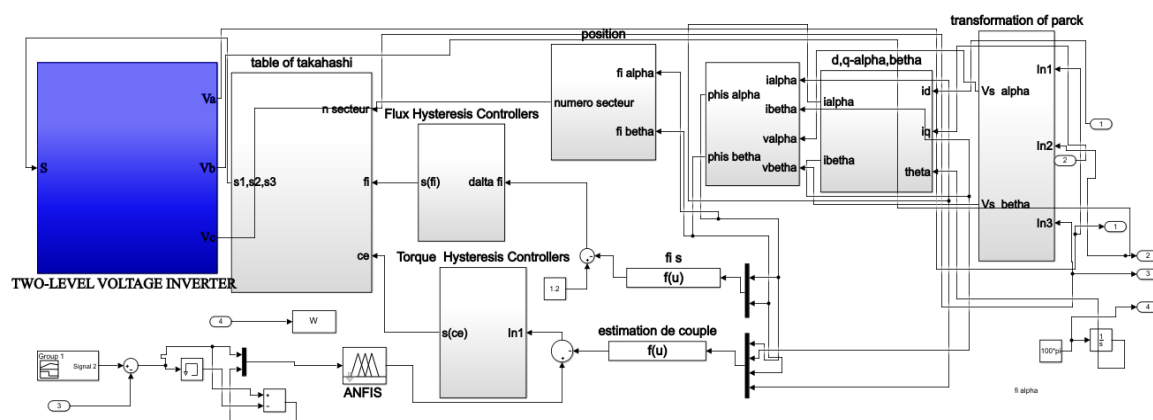


Figure 9. Direct torque control (DTC) model in MATLAB/Simulink

Table 4. Characteristics of the induction machine

Greatness	Value	Greatness	Value
Rated power	1.5 kw	Rotor resistance	3.805 Ω
Rated voltage	220 V	Cyclic stator inductance	0.274 H
Rated speed	1428 rpm	Cyclic rotor inductance	0.274 H
Nominal frequency	50 Hz	Mutual inductance	0.258 H
Rated stator current	3.64 A	Number of pole pairs	2
Stator resistance	4.85 Ω	Moment of inertia	0.031 kg/m ²
Friction coefficients	0.00114 Nm.s/rd		

Figure 10 illustrates the dynamic behavior of the system during the speed range from 0 to 148 rad/s under nominal conditions. At $t = 0.3$ s, the torque resistance is generated by introducing load torque of 10 Nm. The use of Benchmark 1 is essential for evaluating the system's robustness against load fluctuations.

Figure 10(a) depicts the rotor speed response, highlighting a first-order system dynamic. A rapid convergence of the speed towards the reference is observed, with an optimized response time of 0.15 s, demonstrating excellent reactivity. Moreover, the response remains stable, free from unwanted oscillations, ensuring precise and robust tracking of the reference speed.

Figure 10(b) provides a detailed zoom on the rotor speed response between 0.28 s and 0.5 s, corresponding to the introduction of the resistive torque. During this disturbance, a slight decrease of 2.5 rad/s in the reference speed was observed. However, thanks to the system's speed, robustness, and stability, the system instantly corrects this deviation, allowing for a smooth and precise return to the reference speed without noticeable fluctuations.

Figure 10(c) presents the evolution of the stator current. At startup, a significant current peak was observed reaching 35 A in less than 0.1 s, due to the initial inrush current. Subsequently, the current stabilizes and adopts a smooth sinusoidal waveform with slight ripples, reflecting the good dynamic behavior and stability of the system.

Figure 10(d) illustrates the evolution of the electromagnetic torque. At startup, a high peak torque, reaching 40 Nm observed due to the initial acceleration conditions. Subsequently, the torque stabilizes around 0 Nm, with harmonic oscillations ranging between +2.5 Nm and -5 Nm. At $t = 0.3$ s, when a resistive torque of 10 Nm is applied, an instantaneous increase in the electromagnetic torque is observed, allowing the system to compensate for the disturbance. This correction, accompanied by a reduction and readjustment of harmonics, confirms the system's effectiveness in handling load variations. These results demonstrate the excellent robustness of the system, its reactivity to load variations, and its ability to ensure precise reference tracking in steady-state operation, particularly within the framework of Benchmark 1.

Benchmark 2 illustrates the system's behavior at medium speeds, comparing the performance of two control strategies: DTC-ANFIS (solid red curve) and DTC-PI (dashed blue curve). The speed reference follows a trapezoidal profile defined as follows: from 0 s to 0.35 s, the speed reaches +50 rad/s; from 0.35 s to 0.75 s, it drops to 0 rad/s, marking a critical transition phase; and from 0.75 s to 1 s, it reaches -50 rad/s. This speed variation, particularly the zero-crossing phase, provides a relevant test scenario for assessing the accuracy, responsiveness, and robustness of the controllers. Benchmark 2 clearly highlights the ability of both strategies to accurately track the imposed references, while also underlining the advantages of the intelligent ANFIS-based control.

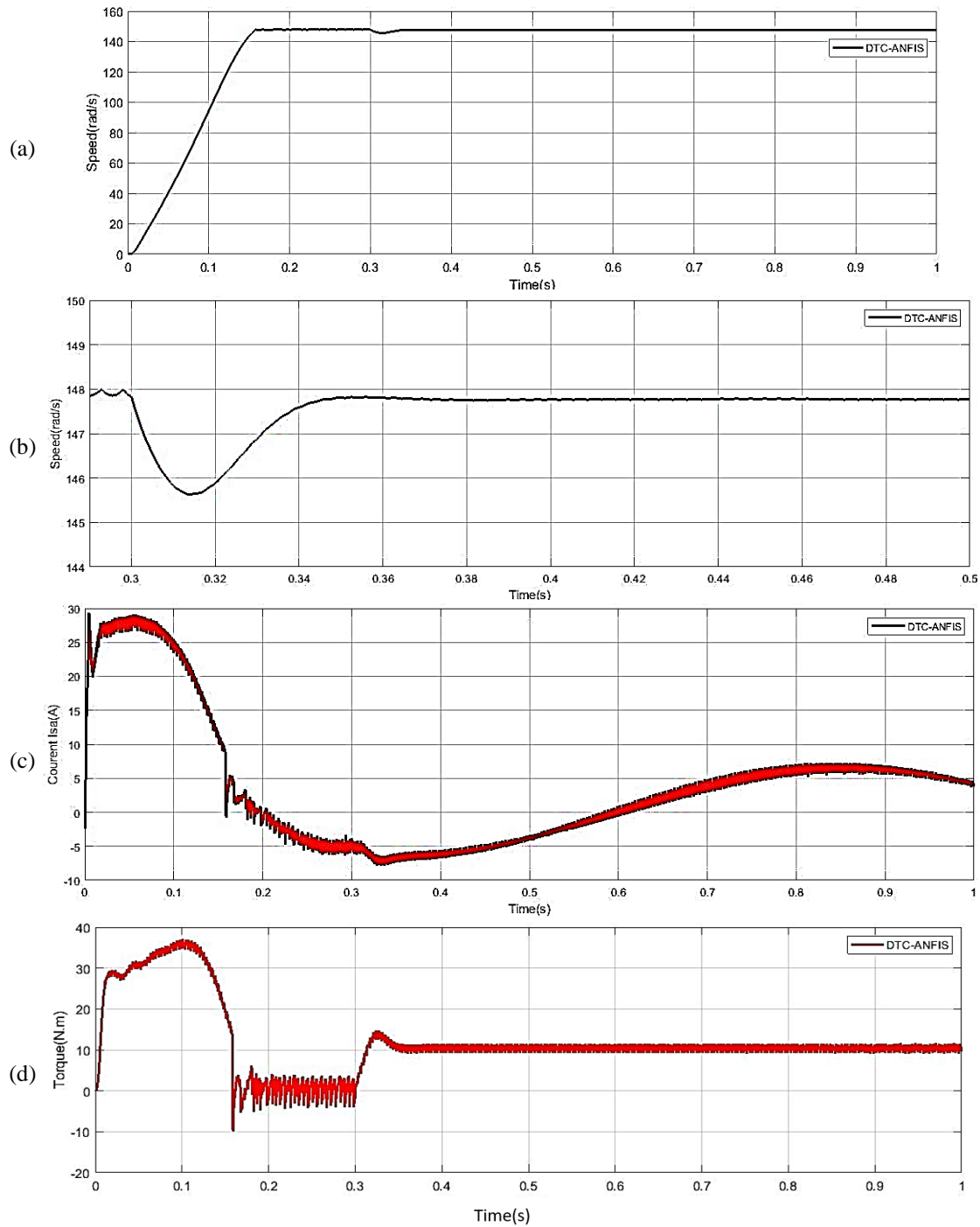


Figure 10. Benchmark 1 trajectory tracking and disturbance rejection performance with the DTC-ANFIS approach for nominal speed: (a) rotor speed response, (b) zoom on the rotor speed, (c) stator current, and (d) electromagnetic torque

Figure 11 shows the response of rotor speed and highlights such performance differences between DTC-ANFIS and DTC-PI. At startup, DTC-ANFIS achieves a rise time of 0.08 s, while DTC-PI requires 0.15 s, demonstrating the faster response of DTC-ANFIS. In steady-state operation, DTC-ANFIS ensures greater stability than DTC-PI, providing precise and reliable reference tracking. In transient mode, DTC-ANFIS enables faster and smoother speed transitions, whereas DTC-PI exhibits less controlled variations. In the third phase of the graph, DTC-PI leads to an unstable system, while DTC-ANFIS maintains excellent stability, confirming its robustness and efficiency in speed control. Table 5 presents a comparison of the mean squared errors (MSE) between the DTC-ANFIS and DTC-PI control strategies, offering an assessment of their performance with regard to accuracy and control efficiency.

Figure 12 presents the electromagnetic torque curves, highlighting the performance differences between the DTC-ANFIS and DTC-PI strategies. During startup, the DTC-PI strategy faces difficulties, as evidenced by its longer startup time of 0.15 s, while the DTC-ANFIS strategy reaches stability in just 0.08 s. Furthermore, the DTC-ANFIS control generates fewer ripples and harmonics compared to the DTC-PI, as shown in Figure 13, confirming its superior efficiency and better control performance. Figure 14 displays the stator current curves. DTC-ANFIS consumes less current than DTC-PI, with reduced harmonic distortion, demonstrating its optimized energy efficiency.

Table 5. Comparison of mean squared errors of DTC-ANFIS and DTC-PI

The speed reference	DTC-PI	DTC-ANFIS
50 rad/s	4.4571	4.2226
0 rad/s	5.4869	4.4972
-50 rad/s	5.1530	4.6824

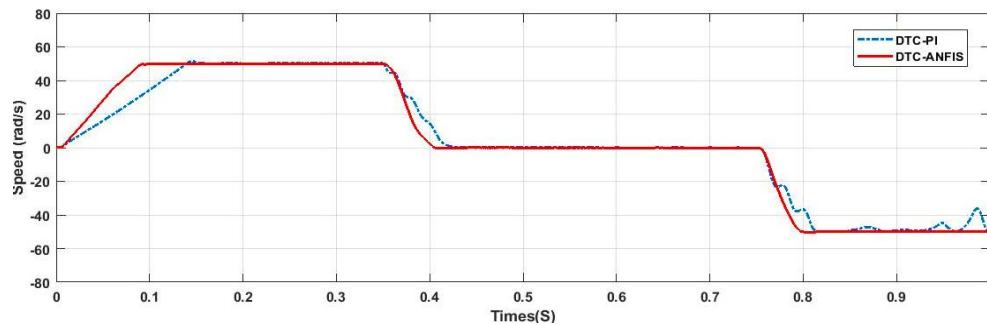


Figure 11. Benchmark 2 - comparison of rotor speed trajectories between DTC-ANFIS and DTC-PI strategies

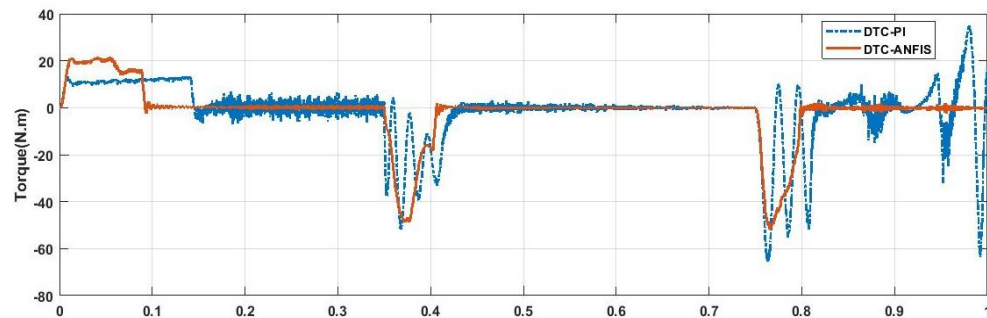


Figure 12. Benchmark 2 - comparison of electromagnetic torque trajectories between DTC-ANFIS and DTC-PI strategies

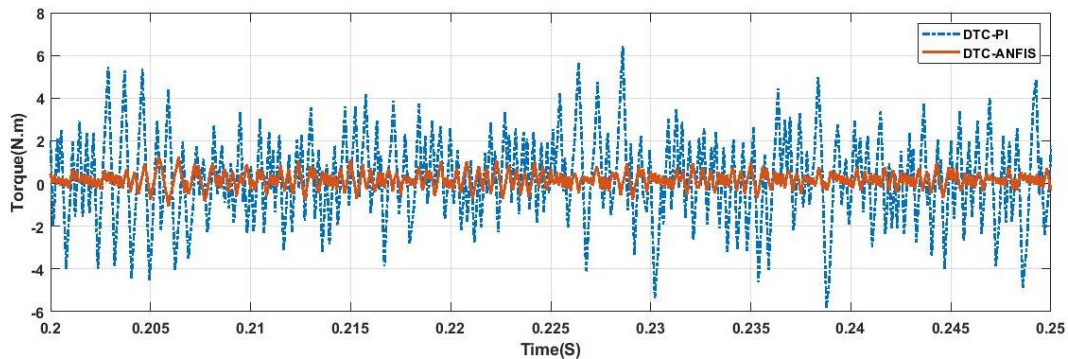


Figure 13. Benchmark 2 - close-up on electromagnetic torque evolution: comparison between DTC-ANFIS and DTC-PI strategies

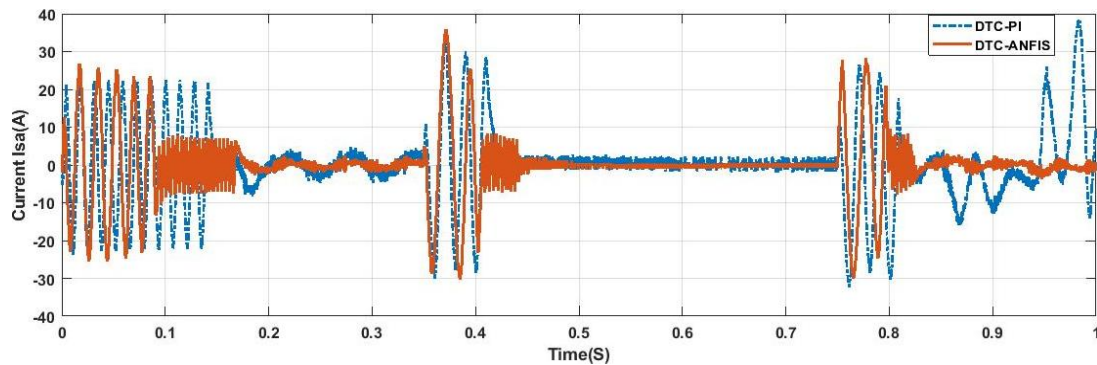


Figure 14. Benchmark 2 - comparison of stator current i_{sa} trajectories between DTC-ANFIS and DTC-PI strategies

4. CONCLUSION

In the following, we suggest an innovative strategy employing the adaptive neuro-fuzzy inference system (ANFIS) to enhance the traditional DTC technique. This approach intelligently adapts the control parameters to optimize DTC performance. To assess the effectiveness of this approach and validate the associated parameters, a series of tests were conducted on two benchmark test benches. The obtained results highlight a significant improvement in the performance of the ANFIS-based controller compared to a conventional DTC using a PI regulator. The effectiveness of this improvement has a direct impact on the behavior of the induction motor, with the following key enhancements: i) Reduction of torque ripples in both transient and steady state conditions, attenuation of motor vibrations, and increased operational lifespan; ii) Minimization of stator current ripples; iii) Fast and robust transient dynamics; and iv) High-precision tracking and stability of the reference speed trajectory. However, the intelligent method has some drawbacks; it requires longer calculation times, and the determination of the database for ANFIS remains complex.

ACKNOWLEDGMENTS

The authors would like to express their sincere gratitude to the Algerian Ministry of Higher Education and Scientific Research for its support and encouragement of academic research.

FUNDING INFORMATION

The authors state that this work was funded by the Mustapha Stambouli University of Mascara, Algeria.

AUTHOR CONTRIBUTIONS STATEMENT

This journal uses the Contributor Roles Taxonomy (CRediT) to recognize individual author contributions, reduce authorship disputes, and facilitate collaboration.

Name of Author	C	M	So	Va	Fo	I	R	D	O	E	Vi	Su	P	Fu
Laoufi Abdelhaq	✓	✓	✓	✓	✓	✓	✓	✓	✓	✓	✓	✓		
Chergui Moulay-Idriss		✓		✓	✓	✓				✓	✓	✓		
Soufiane Chekroun		✓		✓	✓					✓	✓	✓		

C : **C**onceptualization

M : **M**ethodology

So : **S**oftware

Va : **V**alidation

Fo : **F**ormal analysis

I : **I**nvestigation

R : **R**esources

D : **D**ata Curation

O : Writing - **O**riginal Draft

E : Writing - Review & **E**ditng

Vi : **V**isualization

Su : **S**upervision

P : **P**roject administration

Fu : **F**unding acquisition

CONFLICT OF INTEREST STATEMENT

Authors state no conflict of interest.

DATA AVAILABILITY

Derived data supporting the findings of this study are available from the corresponding author, [LA], on request.




REFERENCES

- [1] I. Akkurt, P. Boodaghi Malidarreh, and R. Boodaghi Malidarreh, "Simulation and prediction of the attenuation behaviour of the KNN-LMN-based lead-free ceramics by FLUKA code and artificial neural network (ANN)-based algorithm," *Environmental Technology*, vol. 44, no. 11, pp. 1592–1599, May 2023, doi: 10.1080/09593330.2021.2008017.
- [2] M. T. Çelik and S. Arslankaya, "Analysis of quality control criteria in an business with the fuzzy DEMATEL method: Glass business example," *Journal of Engineering Research*, vol. 11, no. 2, p. 100039, Jun. 2023, doi: 10.1016/j.jer.2023.100039.
- [3] R. B. Malidarreh, I. Akkurt, P. B. Malidarreh, and S. Arslankaya, "Investigation and ANN-based prediction of the radiation shielding, structural and mechanical properties of the Hydroxyapatite (HAP) bio-composite as artificial bone," *Radiation Physics and Chemistry*, vol. 197, p. 110208, Aug. 2022, doi: 10.1016/j.radphyschem.2022.110208.
- [4] S. Gdaim, A. Mtibaa, and M. F. Mimouni, "Artificial neural network-based DTC of an induction machine with experimental implementation on FPGA," *Engineering Applications of Artificial Intelligence*, vol. 121, p. 105972, May 2023, doi: 10.1016/j.engappai.2023.105972.
- [5] O. Alshorman *et al.*, "A review of artificial intelligence methods for condition monitoring and fault diagnosis of rolling element bearings for induction motor," *Shock and Vibration*, vol. 2020, pp. 1–20, Nov. 2020, doi: 10.1155/2020/8843759.
- [6] K. Yung Yap, C. R. Sarimuthu, and J. Mun-Yee Lim, "Artificial intelligence-based MPPT techniques for solar power system: a review," *Journal of Modern Power Systems and Clean Energy*, vol. 8, no. 6, pp. 1043–1059, 2020, doi: 10.35833/MPCE.2020.000159.
- [7] R. Belal, M. Flitti, And M. L. Zegai, "Tuning of pi speed controller in direct torque control of dual star induction motor based on genetic algorithms and neuro-fuzzy schemes," *Revue Roumaine Des Sciences Techniques — Série Électrotechnique Et Énergétique*, vol. 69, no. 1, pp. 9–14, Apr. 2024, doi: 10.59277/RRST-EE.2024.1.2.
- [8] N. El Ouanjli *et al.*, "Modern improvement techniques of direct torque control for induction motor drives - a review," *Protection and Control of Modern Power Systems*, vol. 4, no. 2, pp. 1–12, Apr. 2019, doi: 10.1186/s41601-019-0125-5.
- [9] S. Abouda, F. Nollet, A. Chaari, N. Essounbouli, and Y. Koubaa, "Direct torque control of induction motor pumping system fed by a photovoltaic generator," in *2013 International Conference on Control, Decision and Information Technologies (CoDIT)*, May 2013, pp. 404–408. doi: 10.1109/CoDIT.2013.6689579.
- [10] N. Priyadarshi, S. Padmanaban, J. B. Holm-Nielsen, V. K. Ramachandaramurthy, and M. S. Bhaskar, "An adaptive neuro-fuzzy inference system employed cuk converter for PV applications," in *Proceedings - 2019 IEEE 13th International Conference on Compatibility, Power Electronics and Power Engineering, CPE-POWERENG 2019*, Apr. 2019, pp. 1–5. doi: 10.1109/CPE.2019.8862398.
- [11] I. P. Okokpuje and J. E. Sinebe, "An overview of the study of ANN-GA, ANN-PSO, ANFIS-GA, ANFIS-PSO, and ANFIS-FCM predictions analysis on tool wear during machining process," *Journal Européen des Systèmes Automatisés*, vol. 56, no. 2, pp. 269–280, Apr. 2023, doi: 10.18280/jesa.560212.
- [12] A. M. Ali, M. A. L. Badr, and F. S. Hosain, "Direct torque control of three phase induction motors concept and principles," *Asian Journal of Electrical and Electronic Engineering*, vol. 3, no. 1, pp. 1–15, Apr. 2023, doi: 10.69955/ajoeec.2023.v3i1.40.
- [13] J. Dou, C. Xu, S. Jiao, B. Li, J. Zhang, and X. Xu, "An unsupervised online monitoring method for tool wear using a sparse auto-encoder," *The International Journal of Advanced Manufacturing Technology*, vol. 106, no. 5–6, pp. 2493–2507, Jan. 2020, doi: 10.1007/s00170-019-04788-7.
- [14] M. Konuhova, "Modeling of induction motor direct starting with and without considering current displacement in slot," *Applied Sciences*, vol. 14, no. 20, p. 9230, Oct. 2024, doi: 10.3390/app14209230.
- [15] A. Ahmed, "Real time implementation of fuzzy logic based direct torque control of three phase induction motor," *Przegląd Elektrotechniczny*, vol. 1, no. 2, pp. 102–105, Feb. 2023, doi: 10.15199/48.2023.02.16.
- [16] F. Mansour, "Induction motors: construction, principle of operation, power and torque calculations, characteristics and speed control induction motors: construction, principle of operation, power and torque calculations, characteristics and speed control," *Doi: 10.13140/Rg.2.2.15490.71360 Citation*, vol. 1, no. June, pp. 1–23, 2020.
- [17] A. Azeem *et al.*, "Comprehensive analysis of modulation techniques for two-level inverter," *Lecture Notes in Electrical Engineering*, 2019, pp. 677–688. doi: 10.1007/978-981-13-6772-4_58.
- [18] J. Zheng, C. Peng, K. Zhao, and M. Lyu, "A low common-mode SVPWM for two-level three-phase voltage source inverters," *Energies*, vol. 16, no. 21, p. 7294, Oct. 2023, doi: 10.3390/en16217294.
- [19] N. H. Viet and P. D. Dai, "A comparison of DTC and PTC techniques for induction motor drive systems," in *2021 13th International Conference on Electronics, Computers and Artificial Intelligence (ECAI)*, Jul. 2021, pp. 1–5. doi: 10.1109/ECAI52376.2021.9515130.
- [20] M. Ghibeche, K. Kouzi, D. Difi, and A. Ouanouki, "Investigation of predictive direct torque control of double star permanent magnet synchronous machine (DSPMSM)," *Studies in Engineering and Exact Sciences*, vol. 5, no. 1, pp. 2672–2684, Jun. 2024, doi: 10.54021/seesv5n1-132.
- [21] F. Yang *et al.*, "Improved direct torque control strategy for reducing torque ripple in switched reluctance motors," *Journal of Power Electronics*, vol. 22, no. 4, pp. 603–613, Apr. 2022, doi: 10.1007/s43236-021-00380-z.
- [22] H. Benbouhenni and R. Taleb, "Speed regulator and hysteresis based on artificial intelligence techniques of three-level DTC with 24 sectors for induction machine," *Journal of Renewable Energies*, vol. 20, no. 2, pp. 231–242, Oct. 2023, doi: 10.54966/jreen.v20i2.623.
- [23] A. N. Abdullah and M. H. Ali, "Direct torque control of IM using PID controller," *International Journal of Electrical and Computer Engineering (IJECE)*, vol. 10, no. 1, p. 617, Feb. 2020, doi: 10.11591/ijece.v10i1.pp617-625.
- [24] C. Djamila and M. Yahia, "Direct torque control strategies of induction machine: comparative studies," in *Direct Torque Control Strategies of Electrical Machines*, IntechOpen, 2021. doi: 10.5772/intechopen.90199.
- [25] R. H. Kumar, A. Iqbal, and N. C. Lenin, "Review of recent advancements of direct torque control in induction motor drives - A decade of progress," *IET Power Electronics*, vol. 11, no. 1, pp. 1–15, Jan. 2018, doi: 10.1049/iet-pel.2017.0252.




- [26] N. El Ouanjli, A. Derouich, A. El Ghzizal, A. Chebabhi, M. Taoussi, and B. Bossoufi, "Direct torque control strategy based on fuzzy logic controller for a doubly fed induction motor," *IOP Conference Series: Earth and Environmental Science*, vol. 161, p. 012004, Jun. 2018, doi: 10.1088/1755-1315/161/1/012004.
- [27] M. Elgbaily, F. Anayi, and M. Packianather, "Performance improvement based torque ripple minimization for direct torque control drive fed induction motor using fuzzy logic control," *Control, Instrumentation and Mechatronics: Theory and Practice*, 2022, pp. 416–428. doi: 10.1007/978-981-19-3923-5_36.
- [28] H. F. Rashag, S. P. Koh, A. N. Abdalla, N. M. L. Tan, and K. H. Chong, "Modified direct torque control using algorithm control of stator flux estimation and space vector modulation based on fuzzy logic control for achieving high performance from induction motors," *Journal of Power Electronics*, vol. 13, no. 3, pp. 369–380, May 2013, doi: 10.6113/JPE.2013.13.3.369.
- [29] C. Moraga, "Introduction to fuzzy logic," *Facta universitatis - series: Electronics and Energetics*, vol. 18, no. 2, pp. 319–328, 2005, doi: 10.2298/FUEE0502319M.
- [30] W. J. M. Kickert and E. H. Mamdani, "Analysis of a fuzzy logic controller," in *Readings in Fuzzy Sets for Intelligent Systems*, Elsevier, 1993, pp. 290–297. doi: 10.1016/B978-1-4832-1450-4.50033-X.
- [31] J. Mar and Feng-Jie Lin, "An ANFIS controller for the car-following collision prevention system," *IEEE Transactions on Vehicular Technology*, vol. 50, no. 4, pp. 1106–1113, Jul. 2001, doi: 10.1109/25.938584.
- [32] M. S. Elborlsy, S. A. Hamad, F. F. M. El-Sousy, R. M. Mostafa, H. E. Keshta, and M. A. Ghalib, "Neuro-fuzzy controller based adaptive control for enhancing the frequency response of two-area power system," *Heliyon*, vol. 11, no. 10, p. e42547, May 2025, doi: 10.1016/j.heliyon.2025.e42547.
- [33] J.-S. R. Jang and Chuen-Tsai Sun, "Neuro-fuzzy modeling and control," *Proceedings of the IEEE*, vol. 83, no. 3, pp. 378–406, Mar. 1995, doi: 10.1109/5.364486.
- [34] M. B. Nejad, S. M. Ghamari, and H. Mollaei, "Adaptive neuro-fuzzy inference systems controller design on Buck converter," *The Journal of Engineering*, vol. 2023, no. 10, Oct. 2023, doi: 10.1049/tje2.12316.
- [35] S. Arslankaya, "Comparison of performances of fuzzy logic and adaptive neuro-fuzzy inference system (ANFIS) for estimating employee labor loss," *Journal of Engineering Research*, vol. 11, no. 4, pp. 469–477, Dec. 2023, doi: 10.1016/j.jer.2023.100107.
- [36] A. Kusagur, S. F. Kodad, and B. V. S. Ram, "Modeling, design and simulation of an adaptive neuro-fuzzy inference system (ANFIS) for speed control of induction motor," *International Journal of Computer Applications*, vol. 6, no. 12, pp. 29–44, Sep. 2010, doi: 10.5120/1123-1472.
- [37] M. K. Masood, W. P. Hew, and N. A. Rahim, "Review of ANFIS-based control of induction motors," *Journal of Intelligent & Fuzzy Systems*, vol. 23, no. 4, pp. 143–158, Jun. 2012, doi: 10.3233/IFS-2012-0502.

BIOGRAPHIES OF AUTHORS






Laoufi Abdelhaq    obtained his LMD degree in general electrotechnical engineering in 2012 from the University of Abou Bakr Belkaid, Tlemcen, Algeria. In 2014, he obtained a master's LMD degree in the electrotechnical engineering option in machine control at the University of Abou Bakr Belkaid in Tlemcen, Algeria. Since 2021, he has been a doctoral student in the Automatic Control option of the Machine Control Department of Electrical Engineering, Faculty of Sciences and Technology, University Mustapha Stambouli of Mascara, Algeria. He can be contacted at email: abdelhaq.laoufi@univ-mascara.dz.



Chergui Moulay-Idriss    is a lecturer of the Department of Electrical Engineering, University Mustapha Stambouli of Mascara. obtained a diploma of deepened studies (DEA) in 1993, PARIS-CNAM, magistère in electrotechnics in 1998, University of the USTO-MB Oran, and in 2013 a doctorate in Es-sciences in Electrotechnics, University of the USTO-MB Oran. He can be contacted at email: chergui_cum@yahoo.fr.



Dr. Soufiane Chekroun    was born in Tlemcen, Algeria, in 1983. He received his B.S from the University of Sciences and Technology of Oran-Algeria in 2006 and his M.S. degree from the National School of Oran, ENP-Oran in 2009, and his Ph.D. in Automatic from the University of Sciences and Technology of Oran-Algeria in 2016. Following graduation, he joined the Department of Electrical Engineering of ENP-Oran as a research associate. He is an Associate Professor at the University Mustapha Stambouli of Mascara, Algeria. His research interests include electrical machines, the development of intelligent applications, and the practical developments of high-performance electrical motor drives and their related knowledge control schemes. He can be contacted at email: s.chekroun@univ-mascara.dz.